AJNR

High-Definition Zoom Mode, a High-Resolution X-Ray Microscope for Neurointerventional Treatment Procedures: A Blinded-Rater Clinical-Utility Study

S.V. Setlur Nagesh, V. Fennel, J. Krebs, C. Ionita, J. Davies, D.R. Bednarek, M. Mokin, A.H. Siddiqui and S. Rudin

AJNR Am J Neuroradiol 2019, 40 (2) 302-308
doi: https://doi.org/10.3174/ajnr.A5922
http://www.ajnr.org/content/40/2/302

High-Definition Zoom Mode, a High-Resolution X-Ray Microscope for Neurointerventional Treatment Procedures: A Blinded-Rater Clinical-Utility Study

S.V. Setlur Nagesh, V. Fennel, J. Krebs, C. Ionita, J. Davies, D.R. Bednarek, M. Mokin, A.H. Siddiqui, and S. Rudin

ABSTRACT

BACKGROUND AND PURPOSE: Quality of visualization of treatment devices during critical stages of endovascular interventions, can directly impact their safety and efficacy. Our aim was to compare the visualization of neurointerventional procedures and treatment devices using a 194-μm pixel flat panel detector mode and a 76-μm pixel complementary metal oxide semiconductor detector mode (high definition) of a new-generation x-ray detector system using a blinded-rater study.

MATERIALS AND METHODS: Deployment of flow-diversion devices for the treatment of internal carotid artery aneurysms was performed under flat panel detector and high-definition-mode image guidance in a neurointerventional phantom simulating patient cranium and tissue attenuation, embedded with 3D-printed intracranial vascular models, each with an aneurysm in the ICA segment. Image-sequence pairs of device deployments for each detector mode, under similar exposure and FOV conditions, were evaluated by 2 blinded experienced neurointerventionalists who independently selected their preferred image on the basis of visualization of anatomic features, image noise, and treatment device. They rated their selection as either similar, better, much better, or substantially better than the other choice. Inter- and intrarater agreement was calculated and categorized as poor, moderate, and good.

RESULTS: Both raters demonstrating good inter- and intrarater agreement selected high-definition-mode images with a frequency of at least 95% each and, on average, rated the high-definition images as much better than flat panel detector images with a frequency of 73% from a total of 60 image pairs.

CONCLUSIONS: Due to their higher resolution, high-definition-mode images are sharper and visually preferred compared with the flat panel detector images. The improved imaging provided by the high-definition mode can potentially provide an advantage during neurointerventional procedures.

ABBREVIATIONS: DA = digital angiography; FPD = flat panel detector; HiDef = high definition; PED = Pipeline Embolization Device; RP = reference point

The technologic advances in neuroendovascular devices have led to fluoroscopically guided endovascular treatment of intracranial aneurysms becoming the preferred treatment. The constantly evolving design of stents and coils, and recent development of new technologies such as flow diversion and intrasaccular and bifurcation devices now offer neurointerventionalists a variety of treatment options. However, the commercial x-ray imaging detector technology used during neuroendovascular interventions has not kept up with the increased requirements of image resolution.

The flat panel detector (FPD) used in most angiographic and fluoroscopy suites consists of an array of square pixels based on thin-film transistor technology, with sizes varying from 140 to 200 μm.[1] During the most critical steps of aneurysm treatment, such as deploying or repositioning a stent or flow-diversion devices or manipulating the microcatheter within a coil mass to achieve op-

Received August 21, 2018; accepted after revision November 12.

From the Canon (formerly Toshiba) Stroke and Vascular Research Center (S.V.S.N., J.K., C.I., D.R.B., A.H.S., S.R.), and Departments of Biomedical Engineering (C.I., S.R.), Mechanical and Aerospace Engineering (S.R.), and Electrical Engineering (S.R.), University at Buffalo, State University of New York; Buffalo, New York; Department of Neurosurgery (V.F., J.D.), Gates Vascular Institute at Kaleida Health, Buffalo, New York; Departments of Neurosurgery (S.V.S.N., V.F., C.I., J.D., D.R.B., A.H.S.), Bioinformatics (J.D.), and Radiology (D.R.B., A.H.S., S.R.), Jacobs School of Medicine and Biomedical Sciences, University at Buffalo, State University of New York, Buffalo, New York; Jacobs Institute (J.D., A.H.S.), Buffalo, New York; and Department of Neurosurgery and Brain Repair (M.M.), University of South Florida, Tampa, Florida.

This work was supported by National Institutes of Health grant No. R01EB2873 and equipment support from Canon Medical Systems.

Please address correspondence to Swetadri Vasan Setlur Nagesh, MS, PhD, Canon Stroke and Vascular Research Center, University at Buffalo, 875 Ellicott St, Buffalo, NY 14203; e-mail: ss438@buffalo.edu

Indicates open access to non-subscribers at www.ajnr.org
Indicates article with supplemental on-line table and appendix.
Indicates article with supplemental on-line photos.
Indicates article with supplemental on-line video.
http://dx.doi.org/10.3174/ajnr.A5922

timal coil structure, it is critical to have high-quality images of the treatment area to guide device deployment. To provide such improved imaging, a new detector system (On-line Fig 1) consisting of the conventional large-FOV regular-resolution FPD mode (194-μm pixel size at the detector) and a smaller FOV high-resolution complementary metal oxide semiconductor high definition (HiDef) mode (76-μm pixel size at the detector) has been developed.

Early experience with the HiDef mode in imaging a standard line-pair phantom (On-line Fig 2) demonstrated improved spatial resolution over the standard FPD mode, with line pairs as high as 5.6 line pairs/mm distinctly visualized without loss in information in the HiDef images. However, the objective evaluation of how this new technology with improved performance affects the decision-making during neurointerventional procedures and, specifically, aneurysm embolization with the flow-diversion approach has not been performed. In this study, we present a blinded-rater study comparing the visualization of neurointerventional procedures and treatment devices using the 194-μm pixel FPD and 76-μm pixel HiDef mode of the new-generation x-ray detector system.

METHODS AND MATERIALS

Detector Description

The new x-ray imaging system has both a regular-resolution 194-μm pixel FPD mode and a high-resolution 76-μm pixel HiDef mode in 1 single unit. The FPD mode has larger FOVs, varying from 30 $\times$ 30 cm to 15 $\times$15 cm. Smaller FOVs up to 6.3 $\times$ 6.3 cm are available using digital interpolation. In the high-resolution HiDef mode, only smaller FOVs are available, ranging from 8.9 $\times$ 8.9 to 3.8 $\times$ 3.8 cm.

At any given point in time, 1 of the 2 modes is active, and when needed, the image acquisition between the 2 modes can be quickly changed using an FOV switch, without adding any additional delay to the procedure.

Intervention Model Description

An x-ray image is formed by the differential attenuation of the x-ray beam within a patient's body. During an endovascular neurointervention, the major sources of x-ray attenuation are the human bone (skull) and the soft tissue (including the human cerebral cortex and skin tissue). To simulate this, a neurointervention phantom was developed by placing a human skull (simulating bone attenuation) in-between a total stack of five 1-inch acrylic layers (simulating tissue attenuation[2]). To simulate the cerebral circulation, we embedded a 3D-printed model of patient-based intracranial vasculature, consisting of the internal carotid artery segment, the middle cerebral artery, and the anterior cerebral artery segments closely representing the human circle of Willis region, inside the skull and connected it to a pulsatile flow loop, with water used as circulation fluid. The process of fabricating 3D-printed phantoms was previously described in Ionita et al[3] and Russ et al.[4] The neurointervention phantom setup and its attenuation comparison with 3 commercially available anthropomorphic phantoms are presented in the On-line Appendix.

Neurointerventional Treatment Simulation

For this study, endovascular treatment of intracranial aneurysms of the internal carotid artery with the flow-diversion approach using the Pipeline Embolization Device (PED; Covidien, Irvine, California) was simulated.[5] Five different 3D-printed models with aneurysms in the ICA segment were fabricated and treated with a 4.75 $\times$ 30 mm PED. Due to limitations in the availability of the PED and its high cost, we only partially deployed the device to approximately 50% of its length and then resheathed and reused it for subsequent simulated interventions.

Image Acquisition and Display Setup

The main purpose of the study was to qualitatively evaluate the simulated clinical image sequences of PED deployment acquired using both FPD and HiDef modes of the new detector system. The image acquisitions were divided into the following 2 categories:

Deployment Image Sequences. First, for a particular aneurysm geometry, a PED was partially deployed using a background (bone) subtracted roadmap and an unsubtracted (native) image guidance from 1 of the 2 detector modes (FPD or HiDef). The stent was then resheathed and repositioned to its initial location before deployment. Then, the PED was partially redeployed under road-mapping and native image guidance from the other detector mode. During clinical neurointeventions, the roadmap images and the native images complement each other and are displayed and viewed simultaneously. For comparison, the roadmap images along with the corresponding native images from 1 detector mode form a deployment image sequence.

For the same aneurysm geometry, the 2 deployment imaging sequences, 1 from each detector mode, are considered an image sequence pair.

For a total of 5 aneurysm geometries with 2 C-arm views per geometry (anteroposterior [frontal] and posteroanterior [lateral]), a total of 10 image-sequence pairs under fluoroscopy and 10 image pairs under digital angiography (DA) exposure conditions were obtained. On-line Fig 4 shows frames obtained from a sample image sequence pair acquired under fluoroscopic conditions, and On-line Fig 5 shows frames obtained from a sample image sequence pair acquired under DA conditions. On-line videos 1 and 2 show the PED deployment sequence acquired using HiDef and FPD modes, respectively, for the anatomy and exposure conditions presented in On-line Fig 5.

DSA Image Sequences. For a particular aneurysm geometry, with the PED partially deployed, DSA image sequences using the FPD and HiDef modes each were acquired. 80% iodine and 20% water were used as a contrast agent. Similar to the deployment image sequences, the bone-subtracted image along with the unsubtracted native image from 1 detector formed a DSA image sequence. For the same aneurysm geometry, the 2 DSA image sequences, 1 from each detector, were considered an image-sequence pair.

Ten DSA image sequence pairs were obtained. Similar to On-line Fig 5 (and On-line Fig 4), Fig 1 shows a sample image-sequence pair acquired under DSA conditions.

A 0.3-mm focal spot size and an average geometric magnification of 1.2 were maintained for all the acquisitions. Within an image-sequence pair, the distance between the neurointervention phantom and the detector panel and the view angle (C-arm angle) were kept the same. The exposure conditions as determined by the

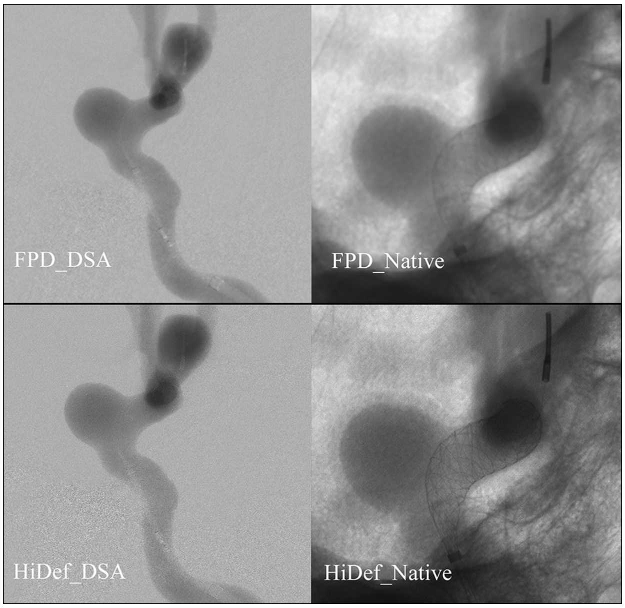

FIG 1. Sample single-image sequence pair acquired under DSA exposures. The average RP air kerma per frame for DSA was calculated to be 1.40 mGy for the FPD mode and 1.34 mGy for the HiDef mode. Due to more quanta reaching the detector, the image quality is improved for both the FPD and HiDef modes compared with On-line Fig 4 and On-line Fig 5. The amount of information available in the HiDef native image is higher than in the FPD native image. For the reader to appreciate the difference between HiDef and FPD images, especially the visualization of the stent, the native images are zoomed-in to the ROI showing the stent area.

automatic exposure control of the imaging system were also kept similar.

For each acquisition, by dividing the cumulative reference-point (RP) air kerma (reported by the angiography machine at a reference point 15 cm from the isocenter toward the x-ray source to approximate the patient entrance air kerma) by the number of frames in the acquisition, we calculated the reference point air kerma per frame. The average of the RP air kerma for both FPD and HiDef modes for fluoroscopy, DA, and DSA acquisitions is reported in the beginning of the Results section.

Image-Quality Evaluation

For rater evaluation, 30 image sequence pairs were acquired, 10 in fluoroscopy, 10 in DA, and 10 in DSA. With each image-sequence pair repeated twice, 60 image-sequence pairs were presented to 2 experienced practicing neurointerventionalist raters. The raters were asked to select their preferred image sequence within a pair based on a comparison of the following 2 criteria—C1: overall image preference in terms of visualization of anatomic features and image noise and C2: the visual quality of the stent.

Different raters can perceive the difference between the images within a pair differently; thus, the raters were asked to score (rater-assigned scores) their selected image as either similar, better, much better, or substantially better than the other image. By means of this rater-assigned score, the detector from which the selected image was acquired was recorded as the preferred detector (detector-preference scores).

Image Display

Two display monitors with the same pixel resolution and similar brightness and contrast levels were used to display the image pairs. For a fair and unbiased comparison, the display monitor stations showing the HiDef and FPD images within an image sequence pair were not the same but were randomized for all the pairs and not made known to the raters.

The detector FOV between the FPD and HiDef modes was kept comparable, 6.3×6.3 cm in the FPD mode and 5.8×5.8 cm in the HiDef mode. The display brightness and contrast between the 2 image sets were adjusted to be similar to avoid any bias. The raters were also free to choose and adjust the display brightness and contrast for each image pair independently. For a fair image comparison, the image processing was kept similar for both HiDef and FPD modes.

Statistical Analysis

For each of the criteria, histogram analysis was performed on the rater-assigned scores as well as the detector-preference score. Intrarater agreement for the rater-assigned scores and interrater agreement for the detector-preference scores for each of the criteria were determined using the binomial exact confidence interval test. Assessment of the degree of agreement was based on the 95% upper confidence values (0–0.49 = poor, 0.50–0.74 = moderate, 0.75–1.0 = good). To establish statistical significance between the FPD and HiDef modes, we conducted a 1-sample *t* test on all rater-assigned scores and the detector preference scores for all criteria. For each of the criteria and all the image pairs, an assumption that both raters would select similar image quality between the 2 detector modes within an image pair was used as the null hypothesis. A P value $< .05$ was considered statistically significant.

RESULTS

The average RP air kerma per frame for fluoroscopy was 0.02 mGy for the FPD mode and 0.03 mGy for the HiDef mode; for DA, it was 0.16 mGy for the FPD mode and 0.17 mGy for the HiDef mode; and for DSA, it was 1.40 mGy for the FPD mode and 1.34 mGy for the HiDef mode.

The histogram distribution of the rater-assigned scores for the 2 criteria for fluoroscopy, DA, and DSA exposures is presented in Fig 2. For fluoroscopic exposures, rater A selected the HiDef images as better than FPD images with a frequency of at least 60% for both criteria, whereas rater B selected the HiDef images as much better than FPD images with a frequency of 50% for both criteria. For DA and DSA exposures, both raters selected the HiDef images as much better than FPD images with an average frequency of 90%.

Combining the rater-assigned scores for both criteria and all 3 exposure modes, both raters, on average, rated the HiDef images as much better than FPD images with a frequency of 73% for both criteria.

The distribution for the detector-preference scores is shown in Fig 3. In all 3 exposure modes for both criteria, both raters preferred HiDef images over FPD images with a frequency of at least 95%.

The results from the binomial exact CI test and 1-sample *t* test are summarized in Tables 1 and 2. For all criteria, both raters had

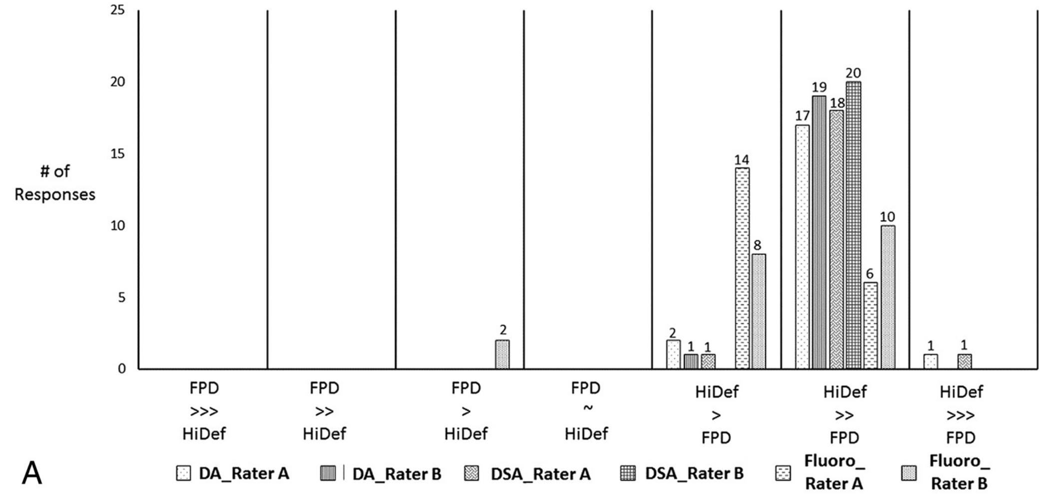

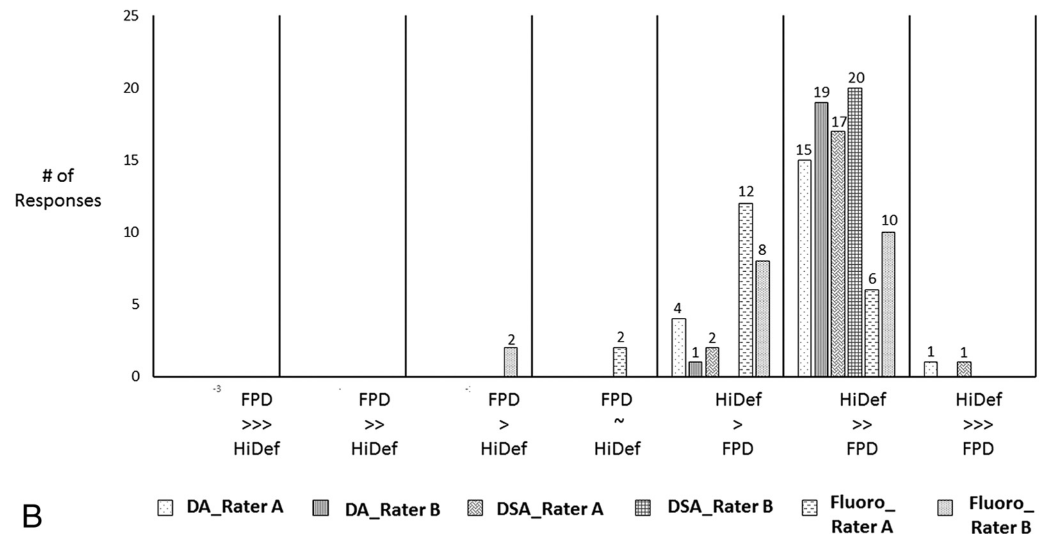

FIG 2. Histogram distribution of rater-assigned scores (raters A and B) for all 5 aneurysm geometries, *A*, The first criterion: overall image preference in terms of visualization of anatomic features and image noise. *B*, The second criterion: visual quality of the stent for all 3 exposure modes: fluoroscopy (Fluoro), DA, and DSA. The raters were asked to score their image preference as either similar (~), better (>), much better (≫), or substantially better (⋙) than the other image.

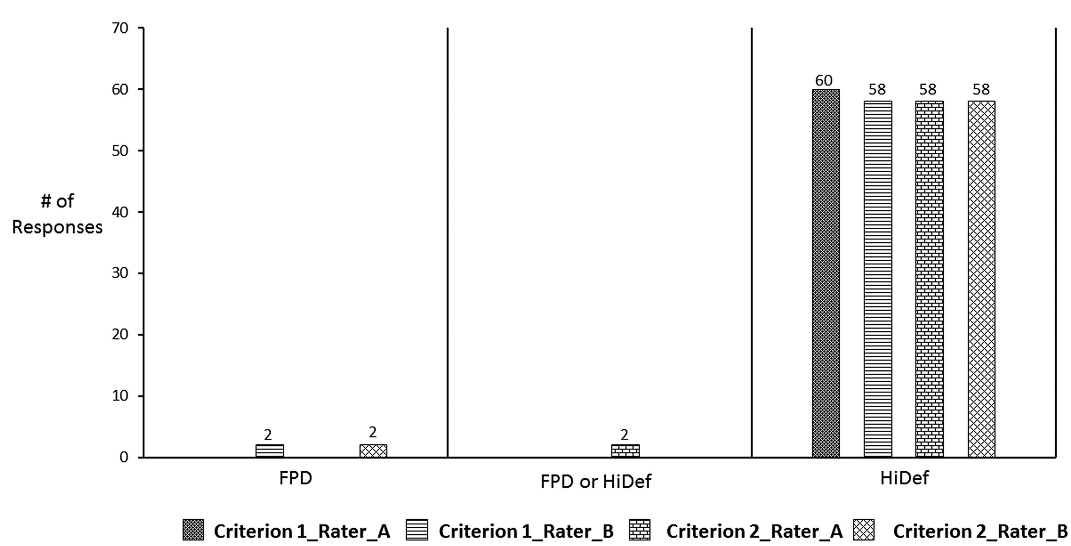

FIG 3. Distribution of detector preference scores for 60 image sequence pairs (all 5 aneurysm geometries) for both criteria. On the basis of the rater-assigned scores (Fig 2), the detector from which the selected image was acquired was recorded as the preferred detector.

Table 1: Statistical test results—binomial exact CI test for intrarater agreement[a]

	Rater-Assigned Scores							
	Intrarater Agreement						1-Sample *T* Test	
	Rater 1			Rater 2				
Criteria	*P*(agr)	95% LC	95% UC	*P*(agr)	95% LC	95% UC	Rater 1 *P* Value	Rater 2 *P* Value
C1	.7	0.50	0.85	.83	0.65	0.94	<.001	<.001
C2	.56	0.37	0.75	.83	0.65	0.94	<.001	<.001

Note:—*P*(agr) indicates probability of agreement; LC, lower confidence; UC, upper confidence; C1, overall image preference in terms of visualization of anatomic features and image noise; C2, the visual quality of stent.
[a] One-sample *t* test for analysis of the scores.

Table 2: Statistical test results—binomial exact CI test for interrater agreement[a]

	Detector-Preference Scores				
	Interrater Agreement			1-Sample *T* Test	
Criteria	*P*(agr)	95% LC	95% UC	Rater 1 *P* Value	Rater 2 *P* Value
C1	.96	0.82	0.99	<.001	<.001
C2	.9	0.73	0.97	<.001	<.001

Note:—*P*(agr) indicates probability of agreement; LC, lower confidence; UC, upper confidence; C1, overall image preference in terms of visualization of anatomic features and image noise; C2, the visual quality of stent.
[a] One-sample *t* test for analysis of the scores.

good intrarater agreement and were consistent. From the detector-preference scores for each criterion, good interrater agreement was determined, further substantiating the results from Fig 3 that both raters generally preferred the HiDef images over the FPD images.

From the 1-sample *t* test for all rater-assigned scores and detector-preference scores for both criteria, a *P* value $< .001$ was calculated for both raters. This indicates that the null hypothesis assumption that the image quality of HiDef and FPD images is similar is wrong and statistically they are significantly different.

DISCUSSION

The improvement in visualization due to use of a surgical microscope was one of the key reasons for its adoption during open craniotomies for treatment of vascular diseases such as brain aneurysms in the late 1960s and 1970s.[6] Similarly, the optimization of laparoscopic visualization has ushered in the standardization of minimalist approaches compared with major open laparotomy procedures during general urologic and gynecologic surgery.[7] Likewise, enhanced visualization during critical aspects of endovascular interventions, such as during microcatheterization and stent or coil deployment, directly impacts the safety and efficacy of neurointerventional procedures.

Previously, high-resolution fluoroscopy systems based on charge-couple devices[8] and complementary metal oxide semiconductors[9] were developed to provide improved imaging of the treatment area compared with existing FPD systems during neurovascular interventions. Successful use of the high-resolution fluoroscopy systems based on charge-couple devices during 2 clinical neurointerventional studies was reported.[10,11] In both cases, high-resolution fluoroscopy provided improved visualization of the endovascular devices. Another study[12] reported that the high-resolution fluoroscopy was particularly beneficial during the treatment of partially thrombosed aneurysms. However, the high-resolution fluoroscopy detector systems were separate from the FPD panels and were mounted on a mechanical changer. Whenever high-resolution imaging was needed, the high-resolution fluoroscopy was deployed into the active FOV using the changer system.

In the new detector system presented in this work, the higher resolution HiDef mode and the regular-resolution mode are available in 1 single unit and can be selected by an FOV switch, which gives it a distinct advantage over the high-resolution fluoroscopy systems. From On-line Fig 2, it can be seen that due to smaller pixel size, the high-resolution HiDef mode has a distinct advantage over the regular-resolution FPD mode and up to 5.6 line pairs/mm can be easily visualized. The aim of our study was to determine whether this added advantage provided by the HiDef mode can actually improve imaging of a treatment device such as a PED, a flow-diverter stent used for the treatment of intracranial aneurysms. When deployed, the PED induces a modification of blood flow within and around the inflow zone of an aneurysm that leads to gradual intra-aneurysmal thrombosis and subsequent atrophy, while preserving flow in the parent vessel and perforating branches.[13]

The subjective assessment of 2 comparable clinical images using image-quality rating scores is a standard practice and has been previously used to compare images from 2 different detectors such as comparing computed radiography with screen films[14] and in comparing selenium-based digital radiography with conventional film-screen (100-speed) radiography.[15]

From the detector-preference score distribution shown in Fig 3, both raters in good agreement (interrater agreement in Tables 1 and 2) preferred the HiDef images over the FPD images for both criteria. For both criteria, from the rater-assigned scores shown in Fig 2, it can be seen that in fluoroscopic exposures, both interventionalists, on average, rated the HiDef image quality as better compared with the FPD quality, whereas in DA and DSA exposures, they rated the HiDef image quality as much better compared with the FPD quality. This is consistent because the image SNR in DA is higher than in fluoroscopy, and in DSA, it is higher than in DA due to increased quanta reaching the detector. During an intervention, it is critical for interventionalists to have optimal visualization of devices such as stents and flow diverters to ascertain their placement along the course of the vessel, ensure proper deployment and wall apposition of the treatment device, and recognize impending kinking or twisting, which can result in unexpected complications.[16]

From On-line Fig 4 acquired in fluoroscopy-exposure conditions, it can be seen that due to higher spatial resolution, visualization of stent and other anatomic features is better in the HiDef mode compared with the regular FPD mode. When we compared

On-line Fig 5 when the PED is deployed with DA with On-line Fig 4 for the same aneurysm geometry, it can be seen that due to higher quanta reaching the detector, while the image quality is improved in both FPD and HiDef images, the amount of information available in HiDef images, especially the visualization of the stent structure including the individual struts, is greater compared with the corresponding FPD image. Such information can be critical during the intervention because devices such as the PED place additional constraints on imaging technology because manipulations during deployment induce changes in the structure of the PED, which may affect treatment outcomes. For instance, with the information provided in HiDef images in On-line Fig 5, one could selectively compress the device to preferentially increase its metal coverage over the aneurysm ostia to induce higher mesh attenuation, aiding occlusion without inducing compression over side branches and perforators, preventing the risk of branch occlusion and postprocedural stroke.[17,18] In the DSA exposure mode shown in Fig 1, the image quality in both FPD and HiDef images is further improved due to higher quanta; however, the information available in HiDef images is much higher than in the FPD images. During the deployment process, a DSA with contrast injection is performed to visualize the flow in the aneurysm and proximal and distal vasculature. With the information in HiDef images, one could visualize the flow not only inside the stent but also around the stent walls in places with poor stent-to-vessel wall apposition.

Furthermore, from the *P* values presented in Tables 1 and 2 for both the rater-assigned and detector-preference scores, it can be deduced that for all criteria, both raters concluded that PED images from the HiDef mode were significantly improved over those from the FPD mode.

Intracranial arteries range from 5 to <1 mm in diameter; and because the treatment devices are continually evolving to enable greater accuracy of treatment in such areas, the imaging technology should also evolve. Flow-diversion devices are being increasingly used for distally located aneurysms with smaller diameter parent arteries.[19,20] With the conventional FPD imaging systems, the images can be digitally interpolated to provide a zoomed-in view of the treatment area and devices when needed. However, the resulting image might still have poor resolution and lower image quality. In the new detector system, when a zoomed-in view is needed, the high-resolution HiDef mode can be turned on electronically. The results of the study show that the HiDef-mode images are significantly improved over the zoomed-in FPD mode. This improvement gives the new detector system a unique advantage over the conventional FPD systems.

The purpose of the study was to evaluate x-ray image quality of the new detector system during neurointerventional treatment. To that extent, the use of a 3D "patient-specific" printed model with appropriate x-ray attenuation simulation can offer a viable alternative to preclinical animal studies. With the advancement in 3D printing technology, an accurate replica of the human vasculature can be easily reproduced. Use of animal studies could provide more information about the actual treatment procedure, such as the biologic interaction of the treatment device and the blood vessels, but this is not within the scope of this work. In this study, we assumed that the treatment would be performed with the patient under general anesthesia, similar to treatment in the study of Nelson et al,[5] thus minimizing patient motion. In both FPD and HiDef modes at high image magnifications, significant patient motion could affect the visibility in background subtracted images due to mask misregistration. Studies involving other neurointerventional treatment devices such as coils, high-porosity stents, and balloons are currently being performed.

CONCLUSIONS

The HiDef mode of the new detector system is equivalent to a microscope that can be used during critical stages of the intervention when superior imaging over the magnified view of the treatment area and devices is required. Due to the high resolution of the HiDef mode, the images are sharper and visually preferred compared with the lower resolution images of the FPD. This is supported by the results of the comparative study presented. Neurointerventions may be performed with a greater degree of accuracy using the improved imaging provided by the new detector system.

Disclosures: Ciprian Ionita—*RELATED*: *Grant*: Canon Medical Systems*; *UNRELATED*: *Consultancy*: Jacobs Institute; *Employment*: University at Buffalo, *Comments*: Assistant Professor; *Grants/Grants Pending*: National Institutes of Health*. Daniel R. Bednarek—*UNRELATED*: *Grants/Grants Pending*: Canon Medical Systems*; *Royalties*: Canon Medical Systems, *Comments*: dose-tracking system licensed through the University at Buffalo Technology Transfer Office.* Maxim Mokin—*UNRELATED*: *Consultancy*: Penumbra, Cerebrotech Medical Systems, Canon Medical Systems. Adnan H. Siddiqui—*UNRELATED*: *Consultancy:* Amnis Therapeutics, Boston Scientific, Canon Medical Systems, Cerebrotech Medical Systems, Cerenovus, Claret Medical, Corindus, EndoStream Medical, Guidepoint Global, Imperative Care, Integra, Medtronic, MicroVention, Northwest University Data and Safety Monitoring Board Chair for the HEAT trial, Penumbra, Rapid Medical, Rebound Therapeutics, Serenity Medical Evaluations, Silk Road Medical, StimMed, Stryker, Three Rivers Medical, VasSol, W.L. Gore & Associates; *Employment*: Jacobs Institute, University at Buffalo Neurosurgery; *Stock/Stock Options*: Amnis Therapeutics, Apama Medical, Blinktbi, Buffalo Technology Partners, Cardinal Health, Cerebrotech Medical Systems, Claret Medical, Cognition Medical, EndoStream Medical, Imperative Care, International Medical Distribution Partners, Rebound Therapeutics, Rist Neurovascular, Serenity Medical, Silk Road Medical, StimMed, Synchron, Three Rivers Medical, Viseon Spine; *Other*: Cerenovus, LARGE trial and ARISE II trial; Medtronic, SWIFT PRIME and SWIFT DIRECT trials; MicroVention, FRED trial and CONFIDENCE study, MUSC POSITIVE trial; Penumbra, Separator 3D Trial, COMPASS trial, INVEST trial, *Comments*: National Principal Investigator/Steering Committees. Stephen Rudin—*RELATED*: *Grant*: Canon Medical Systems, *Comments*: Also, previous work was supported by a grant from National Institutes of Health to the University at Buffalo (Toshiba Medical is now Canon Medical)*; *UNRELATED*: *Patents (Planned, Pending or Issued)*: Canon Medical Systems*; *Royalties*: Canon Medical Systems, *Comments*: coauthor on Dose-Tracking System licensed to Canon by the University at Buffalo.* Jason Davies—*RELATED*: *Grant*: University at Buffalo Clinical and Translational Science Award (CTSA) UL1TR001412 KL2*; *UNRELATED: Stock/Stock Options*: RIST NEUROVASCULAR, INC. *Money paid to the institution.

REFERENCES

1. Nickoloff EL. **AAPM/RSNA physics tutorial for residents: physics of flat-panel fluoroscopy systems—survey of modern fluoroscopy imaging: flat-panel detectors versus image intensifiers and more.** *Radiographics* 2011;31:591–602 CrossRef Medline
2. Schropp L, Alyass NS, Wenzel A, et al. **Validity of wax and acrylic as soft-tissue simulation materials used in in vitro radiographic studies.** *Dentomaxillofac Radiol* 2012;41:686–90 CrossRef Medline
3. Ionita CN, Mokin M, Varble N, et al. **Challenges and limitations of patient-specific vascular phantom fabrication using 3D Polyjet printing.** *Proc SPIE Int Soc Opt Eng* 2014;9038:90380M CrossRef Medline
4. Russ M, O'Hara R, Setlur Nagesh SV, et al. **Treatment planning for image-guided neuro-vascular interventions using patient-specific**

3D printed phantoms. *Proc SPIE Int Soc Opt Eng* 2015;9417 CrossRef Medline
5. Nelson PK, Lylyk P, Szikora I, et al. **The Pipeline Embolization Device for the intracranial treatment of aneurysms trial.** *AJNR Am J Neuroradiol* 2011;32:34–40 CrossRef Medline
6. Uluc K, Kujoth GC, Baskaya MK. **Operating microscopes: past, present, and future.** *Neurosurg Focus* 2009;27:E4 Medline
7. Rassweiler JJ, Teber D. **Advances in laparoscopic surgery in urology.** *Nat Rev Urol* 2016;13:387–99 CrossRef Medline
8. Jain A, Bednarek DR, Ionita C, et al. **A theoretical and experimental evaluation of the microangiographic fluoroscope: a high-resolution region-of-interest x-ray imager.** *Med Phys* 2011;38:4112–26 CrossRef Medline
9. Jain A, Bednarek DR, Rudin S. **Experimental and theoretical performance analysis for a CMOS-based high-resolution image detector.** *Proc SPIE Int Soc Opt Eng* 2014;9033:90333P CrossRef Medline
10. Kan P, Yashar P, Ionita CN, et al. **Endovascular coil embolization of a very small ruptured aneurysm using a novel microangiographic technique: technical note.** *J Neurointerv Surg* 2013;5:e2 CrossRef Medline
11. Binning MJ, Orion D, Yashar P, et al. **Use of the microangiographic fluoroscope for coiling of intracranial aneurysms.** *Neurosurgery* 2011;69:1131–38 CrossRef Medline
12. Starke RM, Turk A, Ding D, et al. **Technology developments in endovascular treatment of intracranial aneurysms.** *J Neurointerv Surg* 2016;8:135–44 CrossRef Medline
13. Eller JL, Dumont TM, Sorkin GC, et al. **The Pipeline embolization device for treatment of intracranial aneurysms.** *Expert Rev Med Devices* 2014;11:137–50 CrossRef Medline
14. Swee RG, Gray JE, Beabout JW, et al. **Screen-film versus computed radiography imaging of the hand: a direct comparison.** *AJR Am J Roentgenol* 1997;168:539–42 CrossRef Medline
15. Piraino DW, Davros WJ, Lieber M, et al. **Selenium-based digital radiography versus conventional film-screen radiography of the hands and feet: a subjective comparison.** *AJR Am J Roentgenol* 1999;172:177–84 CrossRef Medline
16. Mitchell B, Jou LD, Mawad M. **Retrieval of distorted Pipeline embolic device using snare-loop.** *J Vasc Interv Neurol* 2014;7:1–4 Medline
17. Xiang J, Damiano RJ, Lin N, et al. **High-fidelity virtual stenting: modeling of flow diverter deployment for hemodynamic characterization of complex intracranial aneurysms.** *J Neurosurg* 2015;123:832–40 CrossRef Medline
18. Shapiro M, Raz E, Becske T, et al. **Variable porosity of the Pipeline embolization device in straight and curved vessels: a guide for optimal deployment strategy.** *AJNR Am J Neuroradiol* 2014;35:727–33 CrossRef Medline
19. Nossek E, Zumofen DW, Setton A, et al. **Treatment of distal anterior cerebral artery aneurysms with the Pipeline Embolization Device.** *J Clin Neurosci* 2017;35:133–38 CrossRef Medline
20. Puri AS, Massari F, Asai T, et al. **Safety, efficacy, and short-term follow-up of the use of Pipeline Embolization Device in small (<2.5 mm) cerebral vessels for aneurysm treatment: single institution experience.** *Neuroradiology* 2016;58:267–75 CrossRef Medline